

Report Number 11/28

**Growth of confined cancer spheroids: a combined experimental and
mathematical modelling approach**

by

**Loessner, Flegg, Byrne, Hall, Moroney, Clements, McElwain, and
Hutmacher**



Oxford Centre for Collaborative Applied Mathematics
Mathematical Institute
24 - 29 St Giles'
Oxford
OX1 3LB
England

Growth of confined cancer spheroids: a combined experimental and mathematical modelling approach

Loessner D^{1,4*}, Flegg JA^{2,5*}, Byrne HM⁷, Hall CL⁸, Moroney TJ⁵, Clements JA^{1,4}, McElwain DLS^{2,5} and Huttmacher DW^{3,6#}

¹Cancer Research, ²Tissue Repair and Regeneration and ³Regenerative Medicine Programs, Institute of Health and Biomedical Innovation, ⁴Discipline of Cell and Molecular Biosciences and ⁵Discipline of Mathematical Sciences, Faculty of Science and Technology and ⁶Faculty of Built Environment and Engineering, Queensland University of Technology, Brisbane, Australia; ⁷Centre for Mathematical Medicine and Biology, School of Mathematical Sciences, University of Nottingham, Nottingham, England; ⁸Oxford Centre for Collaborative Applied Mathematics, Mathematical Institute, University of Oxford, England.

Running title: Modelling of multicellular cancer spheroids in 3D

Key words: 3D microenvironment, multicellular spheroids, chemoresistance, mathematical modelling

***joint first authors**

#Corresponding author:

Dietmar Huttmacher; Institute of Health and Biomedical Innovation; Queensland University of Technology; 60 Musk Avenue; 4059 Kelvin Grove; Brisbane; Australia

Phone: +61-7-3138-6077; Fax: +61-7-3138-6030; Email: dietmar.huttmacher@qut.edu.au

Introduction

Epithelial ovarian carcinoma (EOC) is the most prevalent aggressive form of ovarian cancer. EOC spreads early by the shedding of malignant cells from the primary ovarian tumour into the peritoneal cavity. These cells then aggregate and form multicellular cancer spheroids within the peritoneal cavity. In the final and most advanced stage, the spheroids then attach themselves to the surface of the peritoneum. They subsequently infiltrate the lining of the peritoneal cavity and metastasise by growing secondary tumours ¹⁻³. *In vitro* experiments involving bioengineered matrices, developed to reflect many of the properties of the *in vivo* situation, have the potential to significantly advance the understanding of cancer spheroid development in ovarian cancer metastasis and other forms of cancer ⁴. In particular, they could assist in elucidating the ways in which biochemical and biomechanical effects combine with intracellular and intercellular signalling to coordinate cancer growth, its interactions with the host stroma and subsequent invasion ⁵. The *in vivo* situation is complex, and therefore there is a compelling need to develop new, physiologically-based *in silico* models that are specialized for particular types of cancers and have the power to generate both qualitative and quantitative predictions about their growth and response to treatment. In addition, certain biophysical parameters which are crucial biomechanical mediators cannot easily be measured experimentally in hydrogel-based microenvironments. In such situations, experimentally-based mathematical models can provide complementary insight and, in so doing, stimulate and guide future experimental work. For example, in a recent review, Kregger and Lauffenburger explained how adopting a systems biology approach can contribute to significant advances in microenvironmental network modelling ⁶.

In addition, the relevance of using two-dimensional cell cultures to increase understanding of tumour growth has been called into question ⁴. A promising alternative involves growing multicellular cancer spheroids in bioengineered three-dimensional (3D) microenvironments, which reflect the *in vivo* situation in a more pathophysiological manner than 2D assays. For example, the growth of cancer cells as 3D aggregates or spheroids confers in them a significant reduction in drug sensitivity and response to radiation ⁷ when compared to traditional monolayer cultures ⁸.

Cell culture models to grow multicellular tumour spheroids in suspension and embedded within naturally derived matrices have long been used to study the responses of tumour cells to exposure to different nutrients, growth factors and/or anti-cancer drugs ^{9,10}. Although these 3D culture systems have enhanced fundamental cancer research, they have experimental limitations. New 3D culture platforms are needed that enable us to replicate the different stages of the *in vivo* growth dynamics of spheroids *in vitro* ^{4,11}.

In this study, we use a bioengineered 3D system based on a peptide-functionalized polyethylene glycol (PEG) hydrogel mimicking the fibrin clot which provides the cancer cell niche in the early phase of ovarian cancer. An advantage of this approach is that, unlike naturally-derived matrices, such as MatrigelTM, the biochemical and mechanical properties of these biomimetic hydrogels can be independently modulated and the material can be manufactured without batch to batch variation ^{12,13}. Replicating the extracellular matrix (ECM) microenvironment using synthetic hydrogels has also been used recently to quantify the proteolytic migration of fibrosarcoma cells. By constructing such a microenvironment, the confounding extracellular influences are limited ¹⁴.

As a cancer model, we have chosen ovarian cancer cells derived from peritoneal ascites (tumour fluid) of EOC. In EOC, resistance to chemotherapy typically occurs. Our bioengineered 3D microenvironment is used to replicate cell–extracellular matrix interactions

that occur during the formation of multicellular cancer spheroids, similar to those found in ascites fluid which accumulates in the peritoneal cavity of patients diagnosed with advanced ovarian cancer^{3,11}. Another important structural component of cancerous microenvironments is the tumour stroma which is rich in fibrin. Fibrin deposited in solid tumours shows parallels to healing wounds¹⁵. Our synthetic hydrogels are formed from multiarm PEG macromolecules via the factor XIII-catalyzed cross-linking mechanism, a reaction occurring during fibrin clot formation in wound healing^{12,13}. Similar processes occurring in the generation of tumour stroma and wound healing result chemically in a water-holding gel¹⁵.

Our experimental 3D work involved the development of biomimetic hydrogels of varying stiffness to grow multicellular spheroids from single cell suspensions encapsulated within these microenvironments and cultured for up to 4 weeks. Immunohistochemistry was used to quantify the dependence of cell proliferation and apoptosis on matrix stiffness, long-term culture and treatment with the anti-cancer drug paclitaxel to obtain experimental data to support mathematical modelling of the growth of multicellular cancer spheroids in these bioengineered 3D microenvironments and their treatment with a therapeutic drug.

In this study, we develop a continuum mathematical model of multicellular spheroid growth. The tumour is viewed as an isotropic and incompressible porous medium¹⁶. We refer to this model as the incompressible porous medium (IPM) model (Figure 1) since multicellular spheroids develop from a single cell in hydrogel-based cultures applied in this work. The IPM model characterises the mechanical properties of the tumour mass via an isotropic pressure and is a natural starting point since it is a simple extension of existing models of 3D growth of tumour spheroids (see, for instance¹⁶). However, when using the IPM model it is not possible to investigate the impact of mechanical effects, other than pressure, on cell proliferation and death.

The IPM model is used to simulate spheroid growth under conditions of different matrix stiffness, culture time and anti-cancer treatment with the chemotherapeutic agent, paclitaxel, an anti-proliferative, cytotoxic drug that stabilizes microtubules of cancer cells. The mathematical model is used to investigate how tumour growth proceeds when the local cell proliferation rate and apoptosis depend on the pressure within the spheroid. The model predictions are in good qualitative agreement with experimental data using markers of proliferation and apoptosis as indicators of cell activity (Figure 1).

Materials and Models

3D cell models

Synthetic hydrogel biomaterials were prepared from peptide-functionalised multiarm polyethylene glycol (PEG) macromolecules. The matrix stiffness was regulated by changing the polymer dry mass of the hydrogel, without changing its biochemical characteristics conferring biomimetic features¹¹. The mechanical properties of the hydrogel were reported previously¹⁷. The human epithelial ovarian carcinoma (EOC) cell line OV-MZ-6 was established from malignant ascites and cultured as described earlier¹¹. For three-dimensional (3D) cell cultures, EOC cells were encapsulated within PEG-based hydrogel precursor solution and cultured for up to 4 weeks to form multicellular spheroids. For exposure to paclitaxel, EOC cell spheroids were grown for 1 week and then treated with paclitaxel (10 nmol/L) for another week. Details of the materials, 3D cultures, immunohistochemistry staining, confocal laser scanning microscopy (CLSM), calculation of cell area and statistical analyses are provided in the supplementary methods.

Mathematical model

The incompressible porous medium (IPM) model that we developed is based on an approach originally proposed by Greenspan¹⁸ and subsequently adapted by many other authors^{16,19,20}. The spheroid is viewed as a radially-symmetric ball of cells, with radius $R(t)$ at time t . By assuming that the tumour mass is incompressible and appealing to the law of mass conservation, it is possible to show that $v(r,t)$, the velocity with which the tumour cells move, is related to the local growth rate via the following equation

$$\nabla \cdot \underline{v} = g(r,t,p) \quad (1)$$

where $g(r, t, p)$ represents the net local growth rate (cell proliferation minus cell death) and is measured in units of volume of growth per unit volume of tissue per time (for details of the assumptions implicit in this model formulation see ¹⁶), p denotes the pressure of the ‘cellular fluid’ within the spheroid, and r denotes the spatial variable (radius). It is assumed that cell movement within the spheroid is governed by Darcy’s Law, so that

$$\underline{v} = -k\nabla p \quad (2)$$

where the constant k represents the ratio of the permeability and the dynamic viscosity. Taken together, equations (1) and (2) give

$$-k\nabla^2 p = g(r, t, p). \quad (3)$$

Under the assumption of spherical symmetry equation (3) becomes

$$\frac{1}{r^2} \frac{\partial}{\partial r} \left(r^2 \frac{\partial p}{\partial r} \right) = \frac{-g}{k}. \quad (4)$$

In equation (4) the growth function g is decomposed into two components, so that

$$g = g_p - g_a$$

where g_p is the proliferation rate and g_a the apoptosis rate. The influence of pressure on cell proliferation and apoptosis is incorporated by employing suitable functional forms for g_p and g_a .

Based on the experimental observation that the proliferation rate appears to be lower in stiffer hydrogels, where we expect the local pressure in the spheroid to be higher, we adopt the following linear form for the dependence of the proliferation/mitosis rate on pressure

$$g_p = s_1^m - s_2^m p, \quad (5)$$

where s_1^m and s_2^m are constants. Again, based on the experimental observation that in a soft hydrogel, where we would expect the local pressure in the hydrogel to be lower, there is a more pronounced apoptotic signal, we adopt the linear form

$$g_a = s_1^a - s_2^a p, \quad (6)$$

where s_1^a and s_2^a are constants. It is remarked that more complex functional forms for g_p and g_a can be investigated, but here the simplest form that captures the experimental observations is employed. Since we have no detailed information on the four constants here we use the following effective pressure dependence of the source/sink of cellular material in the spheroid

$$g = g_p - g_a = (s_1^m - s_1^a) - (s_2^m - s_2^a)p = s_1 - s_2 p$$

Combining equations (4) to **Error! Reference source not found.** supplies the following differential equation for the pressure field within the evolving tumour mass

$$\frac{1}{r^2} \frac{\partial}{\partial r} \left(r^2 \frac{\partial p}{\partial r} \right) = \frac{-(s_1 - s_2 p)}{k}. \quad (7)$$

where $s_1 = s_1^m - s_1^a$ and $s_2 = s_2^m - s_2^a$ are constants. We refer to s_1 as the net growth rate coefficient and to s_2 as the net growth rate linear coefficient.

It is assumed that the outer spheroid radius $R(t)$ moves with the local cell velocity there, so that

$$\frac{dR}{dt} = v(R(t), t) = -k \left. \frac{\partial p}{\partial r} \right|_{r=R}. \quad (8)$$

Equations (7) and (8) are closed by imposing the following boundary and initial conditions. It

is assumed that the tumour spheroid is symmetric about $r = 0$ so that $\left. \frac{\partial p}{\partial r} \right|_{r=0} = 0$.

Furthermore, it is supposed that on $r = R(t)$ the cell pressure balances the restraining force exerted on the growing tumour by the hydrogel. Rather than explicitly modeling the hydrogel (see Chen et al. for a discussion of how this can be done ²¹), it is viewed as a linearly elastic solid and the restraining force, that it exerts on the tumour, is assumed to be proportional to the displacement of material points on the boundary from their initial location, so that

$$p(R(t)) = 4 \frac{\mu}{R_0} (R(t) - R_0), \quad (9)$$

where R_0 is the initial spheroid size and μ the shear modulus of the hydrogel. Further justification for using equation (9) can be obtained by considering the classical problem of a rigid spherical inclusion in an elastic medium ²².

Treatment with paclitaxel

When considering the inhibitory effect of exposure to paclitaxel ²³, it is assumed that the net growth rate coefficient is permanently reduced following treatment which, as in the experimental setup, begins at $t=7$ days. Consequently, in equation (7) the constant s_1 is replaced by the time-dependent function $s_{1,\text{mod}}(t)$, so that

$$s_{1,\text{mod}} = \begin{cases} s_1, & 0 < t < 7 \\ s_0 + (s_1 - s_0)e^{-a(t-7)}, & 7 < t < 14 \end{cases}, \quad (10)$$

where s_1 is the control (non-treated) net growth rate coefficient, the constant a measures how quickly the treatment takes effect, and s_0 is the permanently reduced net growth rate coefficient following treatment (that is $s_0 < s_1$). It is remarked that more complex functional forms for $s_{1,\text{mod}}(t)$ can be employed. For example, if the effectiveness of paclitaxel decreases over time, then the net growth rate coefficient can be assumed to return to its pre-treatment value, s_1 at long times; the consideration of such effects is postponed to future work.

Parameter values

The IPM model contains 7 parameters: s_1 and s_0 are the non-treated and treated net growth rate coefficient respectively, a is the rate of decay from the higher to the lower net growth rate coefficient, s_2 is the net growth rate linear coefficient, R_0 is the initial radius of the spheroid, μ is the shear modulus of the hydrogel and k is the ratio of the permeability to the dynamic viscosity. The constant shear modulus of the hydrogel was taken to be $\mu = 9 \times 10^4$ Pascals²², while the initial radius is taken to be that of a single cell, giving $R_0 = 5 \mu\text{m} = 5 \times 10^{-6} \text{m}$. The parameter k was taken to be $k = 2.2 \times 10^{-13} \text{ m}^3 \text{ day/kg}$. Being highly cell-line specific, the net growth rate coefficient and net growth linear coefficient are determined by inspection to ensure good agreement between the mathematical and experimental values of the spheroid radius after 28 days of culture. These were taken to be $s_0 = 0.5 / \text{day}$, $s_1 = 1 / \text{day}$, $s_2 = 1 \times 10^{-7} / \text{day} / \text{pa}$. Furthermore, $a = 1$ is specified.

Mathematical analysis of the IPM model for growth of a confined non-treated multicellular spheroid

The pressure $p(r,t)$ is determined by integrating equation (7) subject to the boundary conditions at $r = 0$ and $R(t)$ to obtain

$$p(r,t) = A(t) \frac{\sinh\left(\sqrt{\frac{s_2}{k}} r\right)}{r} + \frac{s_1}{s_2}. \quad (11)$$

In equation (11), $A(t)$ is determined from the surface boundary condition, giving

$$A(t) = \left(\kappa(R(t) - R_0) - \frac{s_1}{s_2} \right) \frac{R(t)}{\sinh\left(\sqrt{\frac{s_2}{k}} R(t)\right)}. \quad (12)$$

Substituting (11) and (12) in equation (8) supplies the following ordinary differential equation (ODE) for the spheroid radius $R(t)$

$$\frac{dR(t)}{dt} = -k \left(\kappa(R(t) - R_0) - \frac{s_1}{s_2} \right) \left(\frac{\sqrt{\frac{s_2}{k}} R(t) \coth\left(\sqrt{\frac{s_2}{k}} R(t)\right) - 1}{R(t)} \right), \quad (13)$$

where $\kappa = \frac{4\mu}{R_0}$.

Setting the time derivative to zero in equation (13), it is straightforward to show that the model admits two steady state solutions, \bar{R}_1 and \bar{R}_2

$$\begin{aligned} \bar{R}_1 &= R_0 \left(1 + \frac{s_1}{4s_2\mu} \right), \\ \bar{R}_2 &= 0, \end{aligned} \quad (14)$$

where the nontrivial steady state depends on the elastic properties of the hydrogel *via* the parameter μ , with \bar{R}_1 decreasing as μ increases. This is to be expected since larger values of μ correspond to less compliant (stiffer) hydrogels, which are more resistant to deformation by the expanding tumour spheroid. With our choice of parameter values for R_0, s_1 and s_2 , but leaving μ free, the finding is

$$\bar{R}_1 = 5 \times 10^{-6} + \frac{25}{2\mu}. \quad (15)$$

By linearizing equation (13) about the steady states \bar{R}_1 and \bar{R}_2 , it is straightforward to show that the trivial steady state (spheroid has zero radius) is linearly unstable, while the \bar{R}_1 steady state is linearly stable. It is remarked that for more general choices of g , explicit, closed-form expressions for the steady state solutions do not usually exist. In such cases, a full numerical solution must be computed (see supplementary methods for details).

Results

Spheroid size in response to stiffness of the microenvironment

In order to determine the stress-dependent growth and size of multicellular cancer spheroids embedded within biomimetic hydrogels, the mechanical stress component represented as biomaterial stiffness was varied, by altering the polymer dry mass, from stiff [2.5% (w/v); corresponds to $1201 \pm 121 \text{ Pa}^{11}$], to medium stiff [2.0% (w/v); corresponds to $637 \pm 93 \text{ Pa}^{11}$] and soft [1.5% (w/v); corresponds to $241 \pm 19 \text{ Pa}^{11}$]. Smaller, more compact spheroids were formed in stiff hydrogels, whereas larger and less compact spheroids grew in soft hydrogels (Figure 2A). The proliferative behaviour was also altered due to increasing stiffness. The growth of multicellular spheroids was significantly reduced due to enhanced stiffness (Figure 2B). The area of spheroids, that is the surface area bordered by the cell membranes of the outer cells integrated in a spheroid, correlated with the stiffness of the hydrogels. Significantly smaller spheroids were formed in stiff compared to medium stiff and soft hydrogels (Figure 2C). Spheroids grown in stiff hydrogels showed weak staining for the proteins integrin $\alpha 6$ and Ki67, suggesting low proliferative activity, whereas spheroids grown in soft hydrogels showed strong integrin $\alpha 6$ expression and a distinct Ki67 signal consistent with cells undergoing division in the spheroid centre (Figure 2D; S1; S2). For spheroids cultured in stiff and medium stiff hydrogels, no expression or activation of the apoptotic proteins caspase-3 and caspase-8, and only weak expression of annexin V near the outer spheroid radius were detected. In contrast, for spheroids cultured in soft hydrogels, a more pronounced apoptotic signal, as indicated by cytoplasmic caspase-8 staining near the spheroid periphery, was visualised (Figure 2D; S1; S2).

The evolution of the outer radius of the spheroid was estimated using the mathematical model for four different biomaterial stiffness' (increasing stiffness indicated by increasing values of

$\kappa = \frac{4\mu}{R_0}$) over a defined period of time (2 weeks). The results are illustrated (Figure 2E), with the spheroid radius measured in metres. The IPM model predicted that microenvironments of greater stiffness result in smaller spheroids and this is consistent with our experimental results (Figure 2A-D).

Spheroid size in response to culture time

In the bioengineered 3D microenvironments, spheroids grew significantly in size from 2 to 4 weeks with those at 4 weeks typically having a radius of $147 \pm 5 \mu\text{m}$ (Figure 3A). A distinctive pattern of integrin $\alpha 6$ expression was observed in the spheroid centre after 2 weeks of 3D culture. This was more pronounced after 4 weeks of 3D culture and indicative of continuous proliferative activity and survival within the multicellular spheroids. These spheroids are similar to those found in the ascites fluid that accumulates in the peritoneal cavity of patients with advanced ovarian cancer³. Caspase-8 expression was negligible in spheroids grown for 2 weeks but detected throughout spheroids cultured for 4 weeks indicating that the rates of apoptosis increased with spheroid size (Figure 3A). The proliferation of multicellular spheroids was increased over the monitored time frame of 4 weeks (Figure 3B). The cell area of spheroids, defined as the surface area of the overall spheroid, correlated with the culture time (Figure 3C).

Mathematical modelling was used to simulate the effect of long-term 3D culture (Figure 3D). With our choice of functional forms for the apoptosis and proliferation rates and parameter values, the IPM model predicted a continual increase in the size of the spheroid over a period of 4 weeks. At 2 weeks, the mathematical model predicted an outer spheroid radius of $117 \mu\text{m}$, while by the end of the first 4 weeks, the models reached a steady state of $144 \mu\text{m}$. These results were consistent with our experimental data (Figure 3A, C) and previous long-term 3D

culture results ¹¹. For these results, we used a value of $\mu = 9 \times 10^4$ Pascals and $R_0 = 5 \mu m$, giving a value of $\kappa = 7.2 \times 10^{10} Pa / m$.

Spheroid size in response to anti-cancer treatment

Enhanced cancer spheroid resistance to chemotherapeutics has been observed in patients diagnosed with late stage ovarian cancer ³. We examined the chemoresistance of ovarian cancer cells grown as multicellular spheroids to a clinically-used anti-cancer reagent, paclitaxel. Paclitaxel is a microtubule-stabilizing agent that mediates cell cycle arrest and apoptosis ²³. Ovarian cancer cells were grown for 7 days in biomimetic hydrogels to allow multicellular spheroid formation. The spheroids were then treated with paclitaxel for another week before assessment of cell survival and apoptotic markers was performed. Exposure to paclitaxel led to the formation of more spheroids, although they were smaller in size (radius $45 \pm 5 \mu m$) compared to the non-treated spheroids (radius $76 \pm 7 \mu m$; Figure 4A). Treatment with paclitaxel induced high levels of caspase-8 compared to non-treated cells, indicating enhanced apoptosis and cell death in the treated spheroids (Figure 4A). Due to paclitaxel treatment, the proliferation rate of multicellular spheroids was reduced significantly (Figure 4B). Moreover, exposure to paclitaxel caused significant shrinkage of the total spheroid area [Figure 4C(i)], whereas the overall area of individual cells [Figure 4C(ii)] and the size of their nuclei [Figure 4C(iii)] increased significantly compared to non-treated conditions.

To simulate the effect of treatment with paclitaxel on spheroid growth (shown in blue), the net growth rate coefficient was held constant at $s_1 = 1/\text{day}$, while treatment (shown in red) was assumed to cause exponential decay to a permanently reduced net growth rate coefficient, $s_0 = \frac{s_1}{2}$. Spheroid radii in the non-treated and treated cases diverged after the start of treatment at day 7, with the radii of the treated spheroids after 2 weeks being

approximately $R_f = 117 \mu m$ [Figure 4D(i)]. Treatment reduced the pressure (and, hence, the net growth rate linear coefficient) throughout the spheroid. After treatment, the pressure began to rise again, but not to the levels of the non-treated spheroids [Figure 4D(ii)]. Here we used $\kappa = 7.2 \times 10^{10} Pa / m$.

Discussion

Spheroid size in response to stiffness of microenvironment

Our data showing that microenvironmental stiffness affects spheroid size and expression of survival and apoptotic markers are consistent with other studies. For example, Cheng et al. showed that mechanical stress induced by the microenvironment and cell growth dynamics guided morphological changes in spheroid growth of breast cancer cells by inducing apoptosis, *via* the mitochondrial pathway, in areas of high compressive stress and allowing proliferation in areas of low compressive stress²⁴. In the experiments reported here, ovarian cancer spheroids were smaller and more compact when cultured in stiffer or compressed microenvironments, leading to low levels of expression of apoptotic markers in the spheroid periphery. In our bioengineered matrix, larger and less compact spheroids formed in softer microenvironments and these showed strong staining for markers of cell proliferation and survival (Figure 2A-D; S1, S2).

Helmlinger et al. developed an empirical model to simulate the effects of solid stress on cell proliferation, apoptosis and density²⁵. Cancer cells embedded within agarose gels of varying stiffness formed spheroids that were monitored for up to 6 weeks. The mathematical model focused on linear poroelastic mechanical simulations. Mechanically non-interacting spheroids grew until a growth-inhibitory, threshold level of solid stress was reached²⁵. In line with both our experimental and theoretical results, they observed an inverse correlation between the matrix stiffness and the spheroid growth and size: the stiffer the microenvironment, the fewer and smaller spheroids were formed.

In experimental studies, the proliferation rate was not affected by solid stress, the apoptotic rate decreased and the cellular packing density increased leading to the hypothesis that stress-induced inhibition of tumour growth may confer a survival advantage towards the formation

of a solid tumour. Growth-inhibitory effects were not attributed to limitations in nutrient supply or waste removal in these spheroid cultures. In the same study, it has been also shown that cell–cell contacts are associated with higher cell densities, thereby inhibiting apoptotic events and leading to drug resistance ²⁵.

The constraining effect of the microenvironment was incorporated in the IPM model by assuming that the hydrogel behaves as a linearly elastic material and relating the pressure on the spheroid boundary to the deformation of the matrix. The resulting boundary condition guaranteed an increase in the cell pressure within the spheroid as the radius increases, and captured the hypothesis that the microenvironment itself will be under increasing pressure as the size of the spheroid increases.

Spheroid size in response to anti-cancer treatment

In our experimental investigations, paclitaxel-treated cells revealed morphological features of apoptosis, such as cell shrinkage, nuclear cleavage and chromatin condensation. The application of paclitaxel to cancer spheroids at day 7 of 3D culture was modelled by exponentially reducing the net growth rate coefficient of the spheroids from the time of application. In line with our experiments, the administration of an anti-cancer drug reduced the outer radius of the spheroid in the mathematical simulations.

Our experiments also revealed an increase in caspase-8 expression by the ovarian cancer spheroids with increasing mechanical properties of the microenvironment, culture time and drug treatment. Chen et al. showed that invasive carcinoma cells grown as tumour spheroids embedded in a deformable microenvironment promote caspase-8-dependent and death receptor-independent apoptosis due to disruption of cell–ECM interactions ²¹. The non-apoptotic role of caspase-8 can be caused by post-translational modifications, such as cell

adhesion to the ECM *via* integrins²⁶. Interestingly, caspase-8 expression was detected in the outer region of spheroids grown for 2 weeks, suggesting the presence of dying cells in the spheroid periphery and proliferating cells towards the centre. When spheroids were cultured up to 4 weeks, caspase-8 and integrin $\alpha 6$ expression were detected throughout large spheroids suggesting concomitant and size-dependent expression of both proteins transmitting anti-apoptotic signalling.

In contrast to what was seen in agarose gels²⁵, when ovarian cancer spheroids were cultured for up to 4 weeks in the bioengineered microenvironments, the apoptotic level increased. In the same publication, Helmlinger et al. state that the growth of spheroids cultured in 2.5 mg/mL collagen gels was similarly inhibited when the same experimental setup was used. This result underscores the non-physiological nature of agarose gels although these gels appeared to enable spheroid formation of more aggressive tumour cell lines²⁷.

Differences in material properties used to establish multicellular cancer spheroid cultures of various tumour cell lines are not easily integrated²⁷. Within our biomimetic hydrogel-based microenvironments minor apoptotic events were detectable after 2 weeks, in spheroids of radius of $76 \pm 7 \mu\text{m}$ and became more pronounced in the spheroid centre when radii of $147 \pm 5 \mu\text{m}$ were reached. When spheroids are cultured in agarose gels these apoptotic areas may be replaced by necrosis²⁴.

Strikingly, the overall cell area and size of the cell nuclei were significantly larger in spheroids treated with low doses of paclitaxel than under control conditions. Additionally, and in agreement with published reports^{28,29}, the nuclei of cells used in this study exhibited variable morphologies indicative of apoptotic events (Figure 4A).

Modelling the growth of multicellular cancer spheroids

There has been a concerted effort in developing mathematical models of multicellular spheroids and avascular tumours since Burton viewed tumour growth as a nutrient diffusion problem ³⁰. This work ³⁰ was extended by introducing a surface tension among the living cancer cells and investigating the formation of a central necrotic core and a mechanism to explain the existence of a steady-state tumour size where cell proliferation in the spheroid was balanced by cell death ³¹. Extensive reviews in that area are available from Araujo and McElwain ³², Roose et al. ²⁷ and Byrne ⁵.

The role of stress in tumour development was addressed by using a nonlinear hyperelastic energy function to fit the data on growing spheroids in agarose gels ²⁵. These experiments led to another mathematical model ²¹ where it was suggested that the strain energy function used by Helmlinger et al. ²⁵ does not satisfy the condition of no stress at no strain. A viscoelastic model of residual stresses in a multicellular spheroid was also proposed ³³ while others ³⁴ showed that the stress-related relaxation characteristics of a viscoelastic law may be accommodated by allowing the local growth processes to occur anisotropically. Byrne and Drasdo ¹⁶ compare two different approaches to model multicellular spheroids: an individual cell-based model and a continuum model. An interesting new approach ³⁵ is a triphasic model of tissue growth which takes the ECM, tumour cells and extracellular liquid as the essential constituents.

In this study, we have developed a mathematical model to simulate the growth of multicellular spheroids within a bioengineered matrix. This IPM model was based on an approach originally proposed by Greenspan ¹⁸, where the tumour spheroid can be viewed as an incompressible mass, in which cells follow pressure gradients (Darcy's law). The governing equations are straightforward to solve numerically and we can more readily produce simulations and generate predictions. The spheroid radius was observed to increase from 5 μm to 117 μm over 14 days. Upon treatment at day 7 of spheroid growth, the spheroid

radius was reduced over the time of simulation and the net growth rate coefficient declined exponentially. The model was used to predict the spatial pressure distribution within the spheroid with and without treatment (Figure 4D). The net growth rate linear term was reduced by the administration of treatment.

A comparison between the mathematical models developed by Helmlinger et al.²⁵, Cheng et al.²⁴ and Roose et al.²⁷ and our model is presented in Table 1 with respect to their predictions of the pressure distribution depending on spheroid size, cell proliferation and apoptosis.

Conclusions

We have established a hydrogel-based 3D assay as model system of *in vivo* growth of ovarian tumour spheroids *in vitro*. We have shown that increasing microenvironmental stiffness and exposure to an anti-cancer drug produced smaller spheroids due to increased apoptosis. Our mathematical model captures the experimentally observed results and we can underline that apoptosis-induced cell death relieves the local pressure inside the spheroid and that this allows cells to expand. Our current work forms the basis for the development of a series of new experiments further examining the microenvironmental cues, both extracellular and sub-cellular, affecting tumour cell survival. This extended model will then be used to simulate and incorporate the effects of cancer treatment and chemotherapy resistance dependent on microenvironmental parameters.

Acknowledgements

The authors are grateful to Dr Simone C Rizzi for providing the PEG-based hydrogels and Eva C Weber for her assistance with the immunohistochemistry.

Funding

Support from the National Health and Medical Research Council (NHMRC) of Australia (#553045), the Australian Research Council's (ARC) Discovery Project funding scheme (#DP0878011), an Early Career Research (ECR) Award (#2009001503) from the Queensland University of Technology (QUT) received by DL, a start up grant from QUT for the Chair of Regenerative Medicine, DWH and an Institute of Health and Biomedical Innovation and Discipline of Mathematical Sciences Visiting Research Fellow Award received by HMB are gratefully acknowledged. CLH's work was partly supported by award KUK-C1-013-04, made by King Abdullah University of Science and Technology (KAUST).

Competing interests

The authors have declared that no competing interests exist.

Author contributions

DL and DWH designed, and DL performed the experiments that formed the basis of the mathematical modelling. HMB, JAF, DLSM and CLH developed the mathematical models and JAF and TJM implemented numerical algorithms. JAF performed numerical experiments. DL and JAF wrote, and JAC, DWH, HMB, CLH, TJM and DLSM contributed to the results interpretation, discussion and editorial work of the manuscript.

Abbreviations

CLSM, confocal laser scanning microscopy; ECM, extracellular matrix; EOC, epithelial ovarian carcinoma; IPM, incompressible porous medium; ODE, ordinary differential equation; PEG, polyethylene glycol; 3D, three-dimensional

Figure Legends

Figure 1. Schematic of signalling pathways associated with cell proliferation and apoptosis upon activation of cell surface receptors. Cell–matrix interactions *via* integrins and their associated proteins are essential for signal transduction across the cell membrane for cell function. Integrins mediate proliferative stimuli *via* various signalling cascades reviewed elsewhere and act as cofactors for the stimulation of receptor tyrosine kinases (RTK) ^{36,37}. Apoptotic pathways can be either mediated by intracellular stress signals or by death receptors (FADD) activated by extracellular ligands. Caspases are the final effectors of these apoptotic mechanisms ^{38,39}. The effects of the depicted cell functions are simulated using an incompressible porous medium (IMP) spheroid model.

Figure 2. Cancer cell spheroid formation within hydrogels as a function of biomaterial stiffness. **A.** The growth and size of multicellular spheroids was dependent on a varying stiffness [polymer dry mass percentages 1.5/2.0/2.5% (w/v)] of bioengineered microenvironments depicted by hematoxylin (H)/eosin(E) staining (top panel) and maximal projections of CLSM images (bottom panel; cell actin filaments stained with rhodamine415-conjugated phalloidin red, nuclei with DAPI blue). Large and less compact spheroids grew in less stiff [1.5% (w/v)], and smaller and compact spheroids were formed in stiff [2.5% (w/v)] microenvironments. Scale bars, 20 μ m. **B.** The proliferation of multicellular spheroids, measured as fluorescence per hydrogel condition, was inversely associated with the biomaterial stiffness. Statistical significance, * - $P < 0.05$, ** - $P < 0.01$. **C.** The total cell area of spheroids cultured within matrices of varying stiffness was calculated using Metamorph (integrated morphometry analysis). The spheroid area was inversely correlated with the biomaterial stiffness. Statistical significance, * - $P < 0.05$, ** - $P < 0.01$. **D.** Protein expression

in less stiff microenvironments (1.5% (w/v); left panel) was more pronounced regarding survival stimuli (integrin $\alpha 6$) in the centre and apoptotic (caspase-8) events in outer areas of large spheroids compared to stiff microenvironments (2.5% (w/v); right panel; protein markers stained with respective primary and Alexa488-conjugated secondary antibodies green). Scale bars, 50 μm . **E.** Simulation of spheroid radius as a function of four different stiffness' (increasing stiffness indicated by increasing values of κ (indicated as $\kappa = 7.2 \times 10^{10}$, 7.2×10^{11} , 7.2×10^{12} , 7.2×10^{13}) over a defined period of time (14 days) using the IPM model. This model predicted that higher biomaterial stiffness resulted in smaller spheroid radii.

Figure 3. Protein expression dependent on size and culture time of cancer cell spheroids grown within hydrogels. **A.** Multicellular spheroids grown within bioengineered microenvironments for 2 (left panel) and 4 (right panel) weeks illustrated by H/E staining (top panel) and maximal projections of CLSM images (bottom panel). H/E staining was stronger after 4 weeks in the outer regions of large spheroids (radius $147 \pm 5 \mu\text{m}$). Spheroids formed after 2 weeks (radius $76 \pm 7 \mu\text{m}$) showed a distinctive integrin $\alpha 6$ staining pattern in the spheroid centre and negligible caspase-8 staining. Larger spheroids grown after 4 weeks revealed strong integrin $\alpha 6$ staining throughout the spheroid and some caspase-8 staining scattered in the spheroid centre. Scale bars, 25 μm . **B.** The proliferation of multicellular spheroids, measured as fluorescence per hydrogel condition, was associated with the culture time and significantly increasing over 4 weeks. Statistical significance, ** - $P < 0.01$. **C.** The total cell area of spheroids cultured within hydrogels for 2 and 4 weeks respectively was calculated using Metamorph (integrated morphometry analysis). The spheroid area was significantly increased after 4 weeks in 3D culture compared to 2 weeks. Statistical significance, *** - $P < 0.001$. **D.** Simulation of spheroid radius as a function of culture time (30 days) using the IPM mathematical model. Here we used $\kappa = 7.2 \times 10^{10} \text{ Pa} / \text{m}$.

Figure 4. Behaviour of cancer cell spheroids within hydrogels upon treatment with the anti-cancer drug paclitaxel. **A.** Multicellular spheroids grown within bioengineered microenvironments for 2 weeks without (left panel) or with (right panel) treatment with paclitaxel represented by H/E staining (top panel) and maximal projections of CLSM images (bottom panel). Upon paclitaxel treatment smaller spheroids were formed (radius $45 \pm 5 \mu\text{m}$) compared to non-treated samples (radius $76 \pm 7 \mu\text{m}$). Whereas minor survival stimuli (integrin $\alpha 6$) and increased apoptotic events (caspase-8) were detected after treatment with paclitaxel, a strong integrin $\alpha 6$ expression throughout the spheroid and no caspase-8 expression were visualized without treatment. Scale bars, $25 \mu\text{m}$. **B.** The proliferation of multicellular spheroids, measured as fluorescence per hydrogel condition, was decreased significantly upon paclitaxel treatment. Statistical significance, ** - $P < 0.01$. **C.** The total spheroid area (i) as well as the single cell area (ii) and area of nuclei (iii) of cells grown within a multicellular spheroid were calculated using Metamorph (integrated morphometry analysis). Upon treatment with paclitaxel, the total spheroid area decreased significantly, the single cell area increased significantly and larger nuclei were formed. Statistical significance, ** - $P < 0.01$. **D.** Simulation of spheroid radius (i) and pressure distribution (ii) without treatment (shown in blue) and after treatment (shown in red) using the IPM mathematical model. Exponential growth of the spheroid radius (i) was observed from $5 \mu\text{m}$ (at time $t = 0$) to $117 \mu\text{m}$ (at time $t = 14$ days). Upon treatment at day 7 of spheroid growth, the spheroid radius was reduced over the time of simulation. The pressure level (ii) increased over time without treatment, with the maximum pressure level consistently occurring at the spheroid centre. Upon treatment, the pressure level was reduced, yet continued to rise after the treatment at 7 days, with the maximum pressure level at the spheroid centre. Results were simulated using $\kappa = 7.2 \times 10^{10} \text{ Pa} / \text{m}$.

Figure S1. Proliferative and apoptotic protein expression of cancer cell spheroids grown within medium stiff [2.0% (w/v)] hydrogels. Expression of proliferation (Ki67, integrin $\alpha 6$) and apoptosis (caspase-8) markers of multicellular spheroids were analysed performing maximal projections of CLSM images. A distinct Ki67 staining of a cell undergoing division and transmembrane integrin $\alpha 6$ staining were detected, while cytoplasmic caspase-8 staining was more pronounced at the outer spheroid area. Scale bars, 5 μm .

Figure S2. Cancer cell spheroid formation within hydrogels as a function of material stiffness. **A.** Maximal projections of CLSM images depicted that protein expression in less stiff [1.5% (w/v)] microenvironments was more pronounced regarding survival stimuli (Ki67) in the centre and apoptotic (annexin V, caspase-8) events in outer areas of large spheroids. Scale bars, 50 μm **B.** Protein expression in stiff [2.5% (w/v)] microenvironments was reflected by weak staining of proliferative (Ki67) and apoptotic (annexin V, caspase-8) markers using maximal projections of CLSM images. Scale bars, 50 μm .

Table 1. Comparison between different mathematical models and their predictions of the pressure distribution depending on spheroid size, cell proliferation and apoptosis.

References

1. Permuth-Wey, J. & Sellers, T.A. Epidemiology of ovarian cancer. *Methods Mol Biol* **472**, 413-437 (2009).
2. Sankaranarayanan, R. & Ferlay, J. Worldwide burden of gynaecological cancer: the size of the problem. *Best Pract Res Clin Obstet Gynaecol* **20**, 207-225 (2006).
3. Shield, K., Ackland, M.L., Ahmed, N. & Rice, G.E. Multicellular spheroids in ovarian cancer metastases: Biology and pathology. *Gynecol Oncol* **113**, 143-148 (2009).
4. Hutmacher, D.W., *et al.* Can tissue engineering concepts advance tumor biology research? *Trends Biotechnol* **28**, 125-133 (2010).
5. Byrne, H.M. Dissecting cancer through mathematics: from the cell to the animal model. *Nat Rev Cancer* **10**, 221-230 (2010).
6. Kreeger, P.K. & Lauffenburger, D.A. Cancer systems biology: a network modeling perspective. *Carcinogenesis* **31**, 2-8 (2010).
7. Durand, R.E. & Olive, P.L. Resistance of tumor cells to chemo- and radiotherapy modulated by the three-dimensional architecture of solid tumors and spheroids. *Methods Cell Biol* **64**, 211-233 (2001).
8. Hehlhans, S., Haase, M. & Cordes, N. Signalling via integrins: implications for cell survival and anticancer strategies. *Biochimica et Biophysica Acta* **1775**, 163-180 (2007).
9. Miller, B.E., Miller, F.R. & Heppner, G.H. Factors affecting growth and drug sensitivity of mouse mammary tumor lines in collagen gel cultures. *Cancer Res* **45**, 4200-4205 (1985).
10. Sutherland, R.M. Cell and environment interactions in tumor microregions: the multicell spheroid model. *Science* **240**, 177-184 (1988).

11. Loessner, D., *et al.* Bioengineered 3D platform to explore cell-ECM interactions and drug resistance of epithelial ovarian cancer cells. *Biomaterials* **31**, 8494-8506 (2010).
12. Ehrbar, M., *et al.* Enzymatic formation of modular cell-instructive fibrin analogs for tissue engineering. *Biomaterials* **28**, 3856-3866 (2007).
13. Ehrbar, M., *et al.* Biomolecular hydrogels formed and degraded via site-specific enzymatic reactions. *Biomacromolecules* **8**, 3000-3007 (2007).
14. Schwartz, M.P., *et al.* A synthetic strategy for mimicking the extracellular matrix provides new insight about tumor cell migration. *Integr Biol (Camb)* **2**, 32-40 (2010).
15. Dvorak, H.F. Tumors: wounds that do not heal. Similarities between tumor stroma generation and wound healing. *N Engl J Med* **315**, 1650-1659 (1986).
16. Byrne, H. & Drasdo, D. Individual-based and continuum models of growing cell populations: a comparison. *Journal of mathematical biology* **58**, 657-687 (2009).
17. Klein, T.J., *et al.* Long-term effects of hydrogel properties on human chondrocyte behavior. *Soft Matter* **6**, 5175-5183 (2010).
18. Greenspan, H.P. On the growth and stability of cell cultures and solid tumors*. *Journal of theoretical biology* **56**, 229-242 (1976).
19. McElwain, D.L.S., Callcott, R. & Morris, L.E. A model of vascular compression in solid tumours. *Journal of theoretical biology* **78**, 405-415 (1979).
20. Araujo, R.P. & McElwain, D.L.S. A history of the study of solid tumour growth: the contribution of mathematical modelling. *Bulletin of Mathematical Biology* **66**, 1039-1091 (2004).
21. Chen, C.Y., Byrne, H.M. & King, J.R. The influence of growth-induced stress from the surrounding medium on the development of multicell spheroids. *J Math Biol* **43**, 191-220 (2001).

22. Howell, P., Kozyreff, G. & Ockendon, J. *Applied Solid Mechanics*, (Cambridge University Press, 2009).
23. Ozols, R.F., *et al.* Focus on epithelial ovarian cancer. *Cancer Cell* **5**, 19-24 (2004).
24. Cheng, G., Tse, J., Jain, R.K. & Munn, L.L. Micro-environmental mechanical stress controls tumor spheroid size and morphology by suppressing proliferation and inducing apoptosis in cancer cells. *PLoS One* **4**, e4632 (2009).
25. Helmlinger, G., Netti, P.A., Lichtenbeld, H.C., Melder, R.J. & Jain, R.K. Solid stress inhibits the growth of multicellular tumor spheroids. *Nat Biotechnol* **15**, 778-783 (1997).
26. Barbero, S., *et al.* Caspase-8 association with the focal adhesion complex promotes tumor cell migration and metastasis. *Cancer Res* **69**, 3755-3763 (2009).
27. Roose, T., Netti, P.A., Munn, L.L., Boucher, Y. & Jain, R.K. Solid stress generated by spheroid growth estimated using a linear poroelasticity model small star, filled. *Microvasc Res* **66**, 204-212 (2003).
28. Wang, T.H., *et al.* Paclitaxel (Taxol) upregulates expression of functional interleukin-6 in human ovarian cancer cells through multiple signaling pathways. *Oncogene* **25**, 4857-4866 (2006).
29. Theodoropoulos, P.A., *et al.* Taxol affects nuclear lamina and pore complex organization and inhibits import of karyophilic proteins into the cell nucleus. *Cancer Res* **59**, 4625-4633 (1999).
30. Burton, A. Rate of growth of solid tumours as a problem of diffusion. *Growth* **30**, 157 (1966).
31. Greenspan, H. Models for the growth of a solid tumor by diffusion. *Stud. Appl. Math* **51**, 317-340 (1972).

32. Araujo, R.P. & McElwain, D.L. A history of the study of solid tumour growth: the contribution of mathematical modelling. *Bull Math Biol* **66**, 1039-1091 (2004).
33. MacArthur, B. & Please, C. Residual stress generation and necrosis formation in multi-cell tumour spheroids. *Journal of mathematical biology* **49**, 537-552 (2004).
34. Araujo, R. & McElwain, D. A linear-elastic model of anisotropic tumour growth. *European Journal of Applied Mathematics* **15**, 365-384 (2004).
35. Graziano, L. & Preziosi, L. Mechanics in tumor growth. *Modeling of biological materials*, 263-321 (2007).
36. Schwartz, M.A. & Ginsberg, M.H. Networks and crosstalk: integrin signalling spreads. *Nat Cell Biol* **4**, E65-68 (2002).
37. Cabodi, S., *et al.* Integrin regulation of epidermal growth factor (EGF) receptor and of EGF-dependent responses. *Biochem Soc Trans* **32**, 438-442 (2004).
38. Sato, H., Ogata, H. & De Luca, L.M. Annexin V inhibits the 12-O-tetradecanoylphorbol-13-acetate-induced activation of Ras/extracellular signal-regulated kinase (ERK) signaling pathway upstream of Shc in MCF-7 cells. *Oncogene* **19**, 2904-2912 (2000).
39. Cory, S. & Adams, J.M. The Bcl2 family: regulators of the cellular life-or-death switch. *Nat Rev Cancer* **2**, 647-656 (2002).
40. Mobus, V., *et al.* Morphological, immunohistochemical and biochemical characterization of 6 newly established human ovarian carcinoma cell lines. *International Journal of Cancer* **52**, 76-84 (1992).
41. Landau, H.G. Heat conduction in a melting solid. *Quart. Appl. Math* **8**, 81-94 (1950).
42. Shampine, L.F. & Reichelt, M.W. The matlab ode suite. *SIAM journal on scientific computing* **18**, 1-22 (1997).

Supplementary Methods

Materials. Cell culture reagents, rhodamine415-conjugated phalloidin, Alexa488-conjugated anti-mouse/rabbit IgG, 4'-6-diamidino-2-phenylindole, CyQuant, proteinaseK and ProLong Gold anti-fade reagent were from Invitrogen. Paraformaldehyde, bovine serum albumin and paclitaxel were from Sigma-Aldrich. Polyclonal antibodies anti-annexin V, anti-Ki67, anti-caspase-8 and the monoclonal antibody anti-caspase-3 (#E87) were from Abcam. The monoclonal antibody anti- α 6-integrin (#4F10) was from Chemicon. Triton X-100 was from Calbiochem. TissueTek embedding media and glass coverslips were from ProSciTech.

Three-dimensional cell cultures. Preparation of synthetic hydrogel biomaterials that are formed from peptide-functionalised multiarm polyethylene glycol (PEG) macromolecules *via* the factor XIII-catalysed cross-linking mechanism, a reaction occurring during fibrin clot formation in natural wound healing, was conducted as reported previously^{12,13}. Simultaneously with the hydrogel formation, the RGD integrin-binding motif and a specific cleavage sequence for cell-secreted/activated matrix metalloproteinases (MMP) were incorporated. The matrix stiffness was regulated by changing the polymer dry mass of the hydrogel, without changing its biological and biochemical characteristics conferring biomimetic features. The human epithelial ovarian carcinoma (EOC) cell line OV-MZ-6 was established from malignant ascites and cultured as described earlier⁴⁰. For three-dimensional (3D) cell cultures, EOC cells were encapsulated within PEG-based hydrogel precursor solution and cultured for up to 4 weeks to form multicellular spheroids. For exposure to paclitaxel, EOC cell spheroids were grown for 1 week and then treated with paclitaxel (10 nmol/L) for another week¹¹. Cell spheroids were washed in phosphate-buffered saline (PBS), fixed with 4% (w/v) paraformaldehyde (PFA)/PBS for 20 min at room temperature (RT),

embedded in 50% (v/v) TissueTek/PBS for 40 min at RT, replaced by 100% (v/v) TissueTek for 40 min at RT, frozen in liquid nitrogen and stored at -80°C until cryo-sectioned (5-7 μ m) at the Joint Histo-technology Facility of the University of Queensland and Queensland Institute for Medical Research.

Cell proliferation assays. The growth of multicellular spheroids within PEG-based hydrogels was measured performing CyQuant assays as reported before ¹¹. CyQuant assays and respective fluorescence signals were used to quantify the DNA content per hydrogel. For each condition, three different proliferation assays were conducted in triplicate.

H/E staining. Staining of nuclei with hematoxylin (H) and the cytoplasm with eosin (E) was carried out at the Joint Histo-technology Facility of the University of Queensland and Queensland Institute for Medical Research using standard operation procedures. Photographs were taken using a widefield microscope (LaborLux, Leitz; DXM1200C digital camera with respective ACT-1C software version 1.01, Nikon) with a 40x air objective.

Confocal laser scanning microscopy. After 2 and 4 weeks respectively, F-actin filaments, nuclei and specific cell vitality markers were immunofluorescently stained and imaged by confocal laser scanning microscopy (CLSM). Sections were permeabilised with 0.2% (v/v) triton X-100/PBS for 15 min at RT. Following two washes in PBS, sections were blocked with 1% (w/v) bovine serum albumin (BSA)/PBS for 2 hr at RT. Then, primary (proliferation markers: Ki67 (1/250), integrin α 6 (1/50); apoptotic markers: annexin V (1/250), caspase-8 (1/50), caspase-3 (1/50)) and secondary (Alexa488-conjugated anti-mouse/rabbit IgG (1/1,000)) antibodies in 1% (w/v) BSA/PBS each for 1 hr at RT. The secondary antibody only served as a negative control. F-actin filaments and nuclei were stained with 0.3 U/mL

rhodamine415-conjugated phalloidin and 2.0 $\mu\text{g/mL}$ DAPI respectively in 1% (w/v) BSA/PBS. Sections were mounted with ProLong Gold anti-fade reagent and a glass coverslip. Immunofluorescence was visualized and photographed using a confocal microscope (TCS SP5 II, Leica) with a 20x immersion oil objective. Z-stacks were acquired with a constant slice thickness of 0.5 μm reconstructing a cross-section profile of 5 μm using the Leica Microsystems LAS AF software (version 1.8.2 build 1465) to generate maximal projections.

Calculation of cell area. For overall cell area and nuclei calculations, the integrated morphometry analysis tool in Metamorph (version 7.6.0.0) was used to trace the total spheroid area, the area of single cells within a spheroid and the area of single nuclei using either the phalloidin-stained actin filaments or the DAPI-stained nuclei. Maximal projections using separate channels of CLSM images were arithmetic processed, set to auto-threshold and gray levels binarized. An integrated morphometry analysis was performed to calculate the marked area either of the overall cell area or the nucleus. Averages and standard errors were calculated using Excel (Microsoft, Redmon, WA). For each condition, 5 sections and up to 10 spheroids, single cells or nuclei per spheroid were analysed. For calculation of cell nuclei after paclitaxel treatment, only intact non-lysed cells (without the appearance of apoptotic bodies) were taken into account.

Statistics. Statistical analyses were carried out using a Student's t-test with the software 'R' (version 2.10.0). Results for all analyses with 'P' value less than 0.05 were considered to indicate statistically significant differences (* - $P < 0.05$; ** - $P < 0.01$; *** - $P < 0.001$).

Numerical simulation. To obtain numerical solutions, the growing spatial domain was first mapped onto a fixed domain using the transformation proposed by Landau ⁴¹. Introducing the new spatial variable $X = \frac{r}{R(t)}$, equation (7) was rewritten as

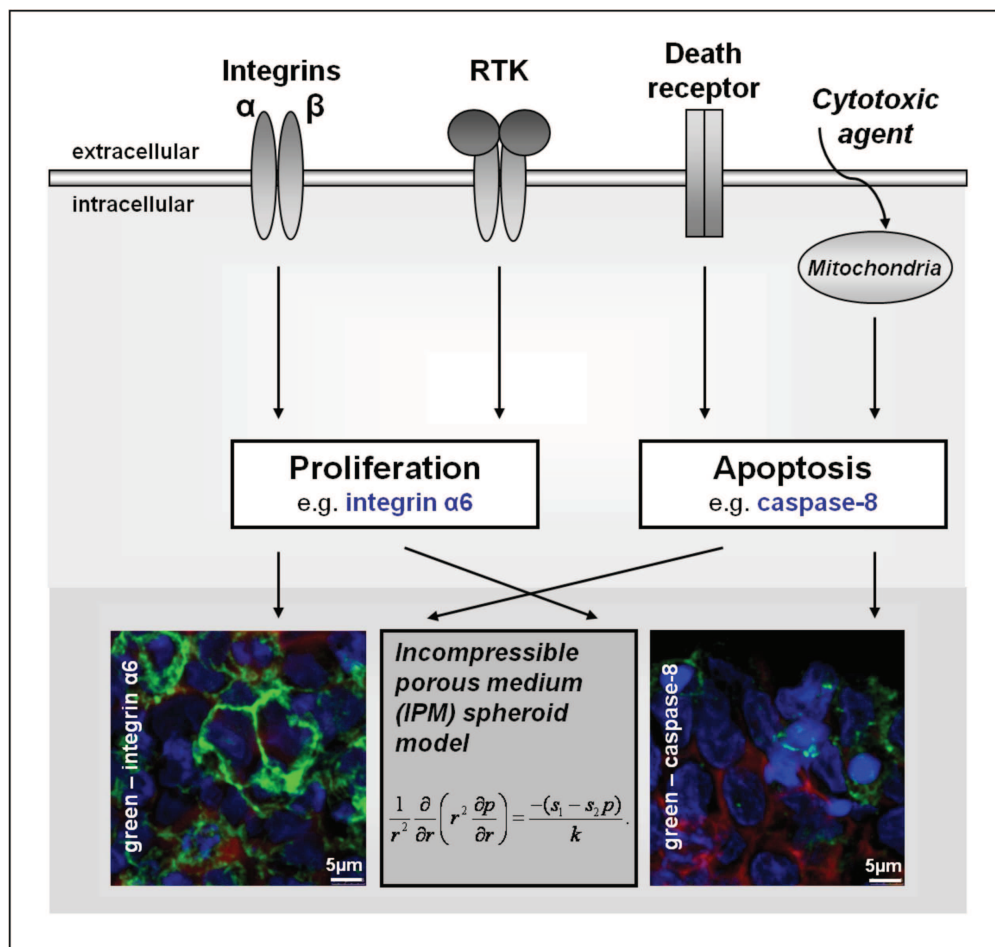
$$\frac{1}{X^2} \frac{\partial}{\partial X} \left(X^2 \frac{\partial p}{\partial X} \right) = \frac{-R(t)^2 (s_1 - s_2 p)}{k} \quad (16)$$

where the domain of simulation was now $X \in [0,1]$. The equation for the moving boundary was similarly transformed to give

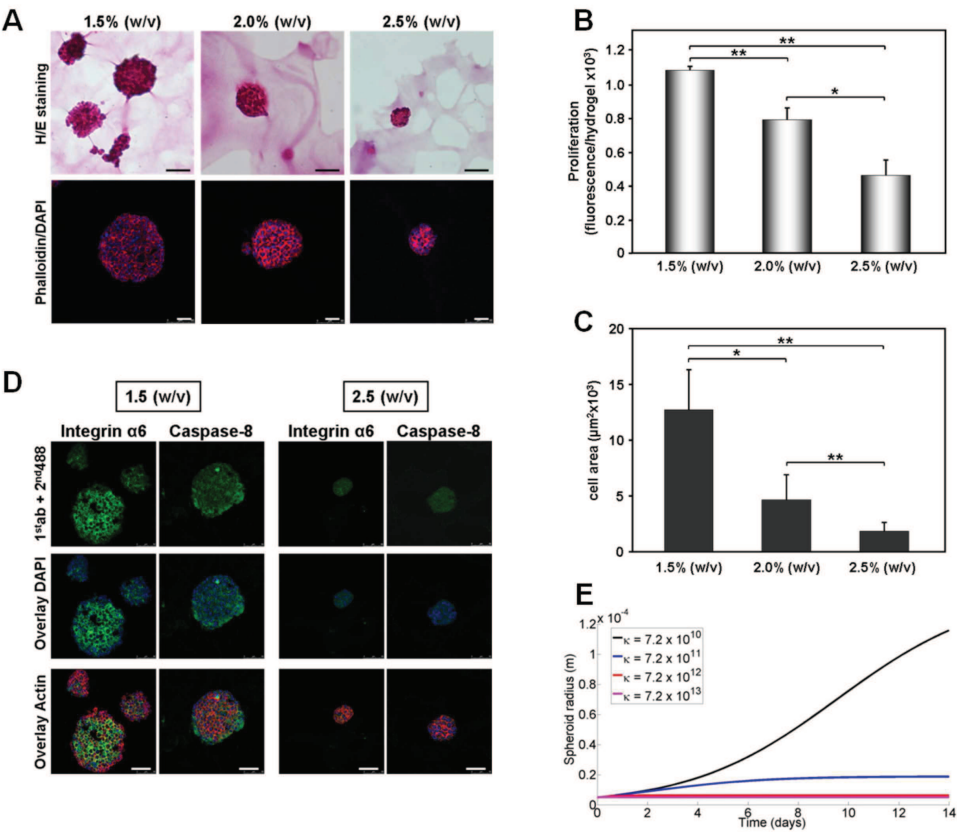
$$\frac{dR}{dt} = -\frac{k}{R(t)} \frac{dp}{dX}. \quad (17)$$

Introducing a uniform mesh over the domain $[0,1]$, and using standard second-order central-difference approximations for the spatial derivatives, (16) was discretised to yield an algebraic system of equations for the pressure at each mesh node. At the inner node, the symmetry boundary condition was applied in the standard way to remove the artificial singularity. At the outer node, the Dirichlet boundary condition (9) was imposed.

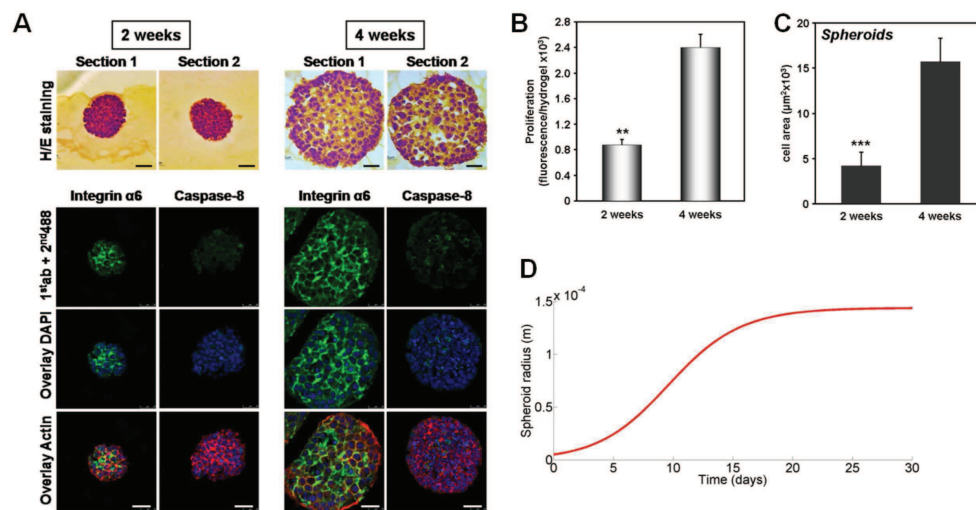
The resulting algebraic system was coupled with the ordinary differential equation (17) and solved using MATLAB's stiff differential/algebraic equation (DAE) solver 'ode15s' ⁴². Having obtained the numerical solutions on the fixed grid, the results were mapped back to the growing domain $0 \leq r \leq R(t)$ for visualisation.



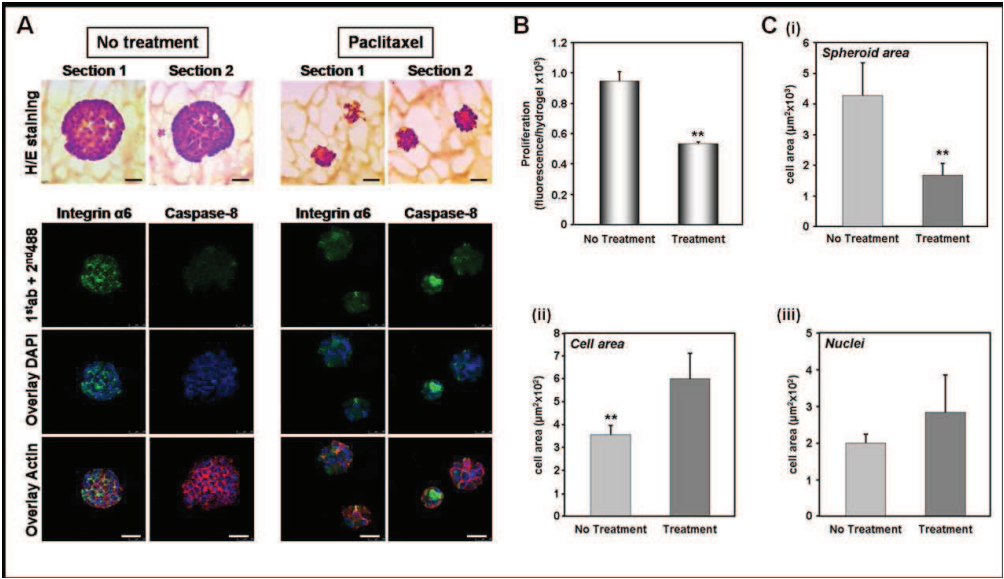
215x203mm (300 x 300 DPI)



215x184mm (300 x 300 DPI)



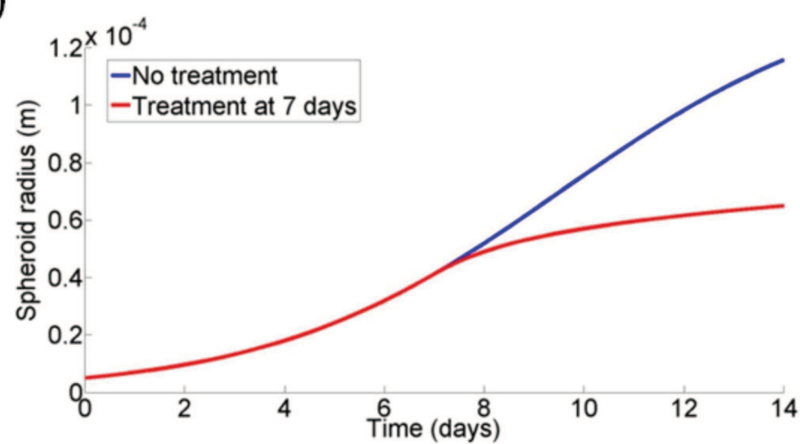
215x117mm (300 x 300 DPI)



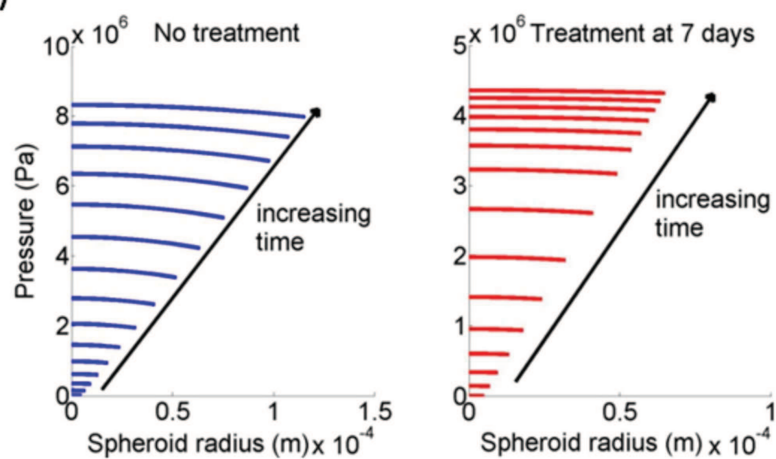
215x123mm (150 x 150 DPI)

D

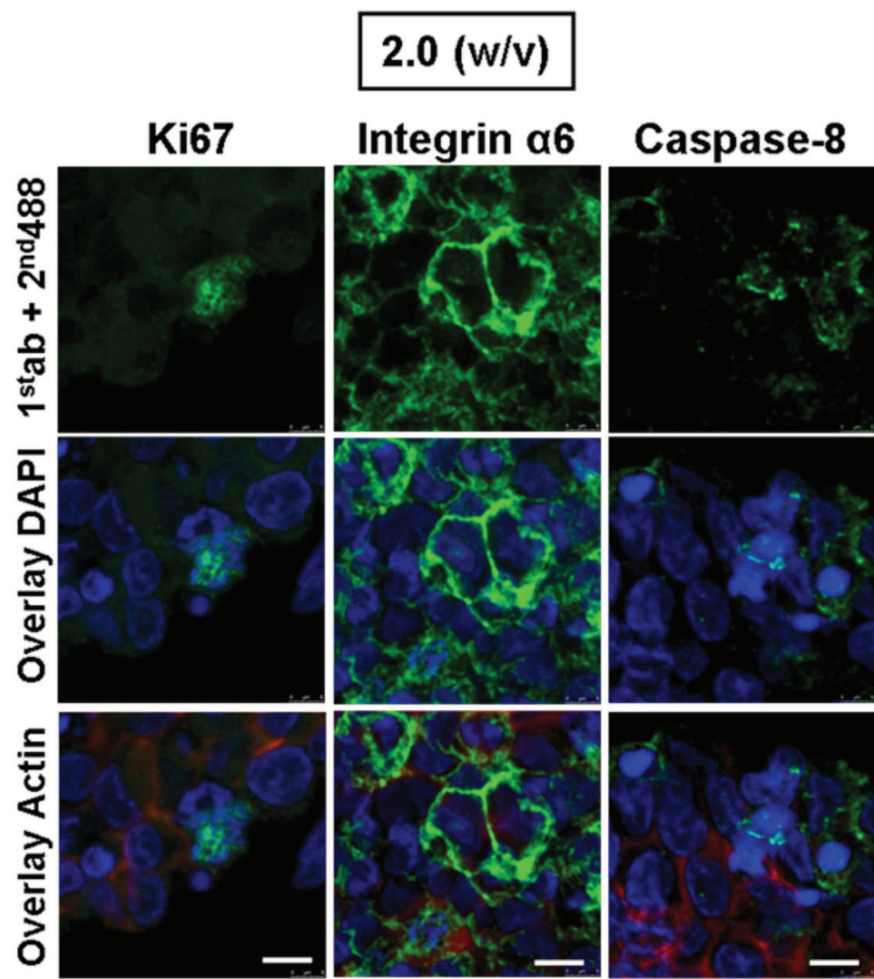
(i)



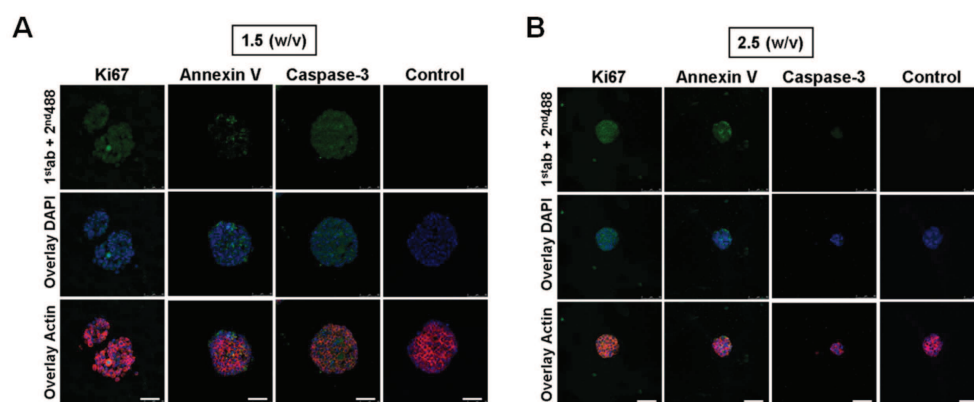
(ii)



215x256mm (300 x 300 DPI)



215x230mm (300 x 300 DPI)



215x93mm (300 x 300 DPI)

Reference; Publication; Cell type Increasing stress caused change to:	Helminger et al. (Nat Biotechnol, 1997) [25] human colon adenocarcinoma cells (LS147T); rat rhabdo- myosarcoma cells (BA-HAN-1); murine mammary carcinoma cells (MCAIV)	Cheng et al. (PLoS One, 2009) [24] non-metastatic murine mammary carcinoma cells (67NR); metastatic murine mammary carcinoma cells (EMT6)	Roose et al. (Microvasc Res, 2003) [27] human melanoma cells (Mu89); mouse melanoma cells (B16F1, B16F10)	Loessner et al. (current study; Biomaterials, 2010) [11] human epithelial ovarian cancer cells (OV-MZ-6)
Cell number; Culture system; Culture time (days); Shear modulus (Pa)	single cell/1-inch inserts for 34 days; 0.5/0.7/0.8/0.9/1.0%(w/v) agarose gels; $G' = 6/14/13.3/16/6.7 \times 10^3 \text{ Pa}$	hanging droplets of 3.0×10^5 67NR cells/ml, 2.0×10^5 EMT6 cells/ml for 3 days; 3.5×10^3 cells/ml embedded in 0.5/1.0%(w/v) agarose gels for 45 days; $G' = 4/7 \times 10^3 \text{ Pa}$	10^4 cells/ml (single cell suspension) for 20 (up to 60) days; 0.5/1.0%(w/v) agarose gels; $G' = 6/6.7 \times 10^3 \text{ Pa}$	0.35x10 ⁵ cells/ml (single cell suspension) embedded within hydrogels for 14 days; 1.5/2.0/2.5%(w/v) polymer dry mass corresponds to $G' = 241 \pm 19/637 \pm 93/1201 \pm 121 \text{ Pa}$
Total spheroid size (μm)	0.5%(w/v): 414 μm 0.7%(w/v): 370 μm 0.8%(w/v): 360 μm 0.9%(w/v): 200 μm 1.0%(w/v): 85 μm decreased	hanging droplets: 300 μm embedded spheroids: 0.5%(w/v): 250 μm 1.0%(w/v): 50 μm	cells grow 1.125 times larger in 0.5%(w/v) than 1.0%(w/v) agarose gel; 0.5%(w/v): 27 μm 1.0%(w/v): 24 μm decreased	1.5%(w/v): $12.7 \times 10^4 \mu\text{m}^2$, 128 μm 2.0%(w/v): $4.7 \times 10^3 \mu\text{m}^2$, 76 μm 2.5%(w/v): $1.8 \times 10^3 \mu\text{m}^2$, 49 μm
Cell spheroid size	decreased	decreased	decreased	decreased
Cell proliferation	LS147T: solid stress up to 1% agarose, while inhibiting macroscopic spheroid growth did not affect net proliferation rate; similar results for BA-HAN-1 and MCAIV spheroids	decreased; suppressed in direction of high mechanical stress	neither: nutrient dependent	decreased
Cell apoptosis	decreased(TUNEL); exclusively in central region	increased; central	neither: constant term	decreased
Question marks	decrease in cell apoptotic rate and spheroid size explained by an increase in cell density; cell seeding density?	shear modulus for 1.0%(w/v) not determined because sample volume was too small	spheroid size reduced	cell density morphoelasticity not modelled

RECENT REPORTS

05/11	Solving Eigenvalue problems on curved surfaces using the closest point method	MacDonald Brandman Ruuth
06/11	A numerical methodology for the Painleve equations	Fornberg Weideman
07/11	Strong stability preserving two-step Runke-Kutta methods	Ketcheson Gotlieb MacDonald
08/11	Hysteresis and Post Walrasian Economics	Cross McNamara Kalachev Pokrovskii
09/11	A locally adaptive time-stepping algorithm for petroleum reservoir simulations	McNamara Bowen Dellar
10/11	On the predictions and limitations of the BeckerDoring model for reaction kinetics in micellar surfactant solutions	Griffiths Bain Beward Colegate Howell Waters
11/11	Dynamics of the Tear Film	Braun
12/11	The infuence of receptor-mediated interactions on reaction-diffusion mechanisms of cellular self-organisation	Klikaa Baker Headon Gaffney
13/11	Quasi-steady state analysis of two-dimensional random intermit-tent search processes	Bressloff Newby
14/11	A Constrained Approach to Multiscale Stochastic Simulation of Chemically Reacting Systems	Cotter Zygalakis Kevrekidis Erban
15/11	The Two Regime Method for optimizing stochastic reaction-diffusion simulations	Flegg Chapman Erban
16/11	Recombination via tail states in polythiophene:fullerene solar cells	Kirchartz Pieters Kirkpatrick Rau Nelson
17/11	Energy versus electron transfer in organic solar cells: a comparison of the photophysics of two indenofluorene: fullerene blend films	Soon Clarke Zhang Agostinelli Kirkpatrick Dyer-Smith McCulloch

21/11	A novel model for one-dimensional morphoelasticity. Part I: Theoretical foundations	Hall Menon McCue McElwain
22/11	A novel model for one-dimensional morphoelasticity. Part II: Application to the contraction of fibroblast-populated collagen lattices	Hall Menon McCue McElwain
23/11	Positive or negative Poynting effect? The role of adscititious inequalities in hyperelastic materials	Mihai Goriely McCue McElwain
24/11	On approaches to modelling lattice dislocations	Hall Markenscoff
25/11	Nonlinear waves in heterogeneous elastic rods via homogenization	de Luna Emptage Goriely Bressloff
26/11	Synaptic bistability due to nucleation and evaporation of receptor clusters	Burlakov Duričković Goriely
27/11	Particle trapping and banding in rapid solidification	Elliot Peppin

Copies of these, and any other OCCAM reports can be obtained from:

**Oxford Centre for Collaborative Applied Mathematics
Mathematical Institute
24 - 29 St Giles'
Oxford
OX1 3LB
England
www.maths.ox.ac.uk/occam**